Acta Mech 234, 5331–5347 (2023)
https://doi.org/10.1007/s00707-023-03651-x

ORIGINAL PAPER

Xiang Mu · Wenshuai Xu · Zhaowei Zhu · Liangliang Zhang · Yang Gao

Image force in cubic piezoelectric quasicrystal half-space and bi-material composite space

Received: 24 February 2023 / Revised: 3 June 2023 / Accepted: 25 June 2023 / Published online: 31 July 2023

Abstract This paper is concerned with the image force in cubic piezoelectric quasicrystal semi-infinite space and infinite space containing two dissimilar quasicrystal half-spaces. On the basis of the Stroh formalism, the expressions of the Green's function for generalized displacement and stress under multi-physical loading conditions are obtained exactly. Also, the image force applied to a generalized line dislocation with different boundary conditions is taken into account. The image force for the traction-free and electrically open surface always attracts dislocation to the boundary, while that for clamped and electrically closed surface shows the opposite tendency. Illustrative examples, such as generalized line force and line charge, are given to present the mechanical behaviors of quasicrystals under different loading conditions and investigate the influences of material parameters and dislocation scheme on image force. The results show that generalized line force has little effect on atomic configurations, and image force F is the strongest when phonon and phason dislocations interact together.

1 Introduction

The interaction between the dislocation and boundary, which is usually described as image force, is an important factor affecting the mechanical behaviors of solids [1]. Asaro [2] discussed the image force between a semi-infinite crack and a straight dislocation and found that it was not dependent on the dislocation's angular position. Ting and Barnett [3] investigated the image force in an anisotropic elastic half-space with a free or fixed boundary as well as bi-material. Lubarda [4] examined the image force produced by the free surface of a cylindrical void on a nearby straight dislocation under mixed type and got the expressions for the glide and climb components. However, to the authors' knowledge, these studies are related to crystal material, not quasicrystals (QCs). The image force of QCs is more complex than that in traditional crystal materials because of the existence of phonon and phason fields.

QCs possess long-range ordered structures, which were firstly found in Al–Mn alloy experiments by Steinhardt et al. in 1984 [5]. Up to now, there are more than 100 dissimilar metal alloy systems available for

X. Mu · Z. Zhu · L. Zhang (✉) · Y. Gao (✉)
College of Science, China Agricultural University, Beijing 100083, China
e-mail: llzhang@cau.edu.cn

Y. Gao
e-mail: ygao@cau.edu.cn

X. Mu
College of Engineering, China Agricultural University, Beijing 100083, China

W. Xu
Key Laboratory of Microgravity, Institute of Mechanics, Chinese Academy of Sciences, Beijing 100190, China

W. Xu
University of Chinese Academy of Sciences, Beijing 100049, China

QC phases. As a result of their unique atomic arrangements, QCs possess numerous desirable properties, such as corrosion resistance, oxidation resistance, and non-stick properties [6]. Based on these, QCs can be used for hydrogen storage tank, solar thin film materials, sensors, and composite reinforcement phases [7].

Piezoelectric effect has a wide range of applications in electronic technology, such as sensors and actuators. Before the piezoelectric effect in QCs was discovered, great efforts have been contributed to piezoelectric material [8, 9]. By virtue of the finite element method, Zhu and Liu [10] took into account three-dimensional (3D) planar crack and non-planar defects of piezoelectric materials. By means of the Stroh formalism, Wang [11] established the relationship between the size of the strip saturation zone ahead of a crack tip and the applied electric displacement field. Chen [12] explored the singularities of piezoelectric bonded wedges which are subjected to thermal effect under mixed boundaries using generalized Lekhnitskii formulation and Mellin transform. Yu et al. [13] obtained the stress intensity factors and electric displacement intensity factor with complex interfaces for nonhomogeneous piezoelectric materials. These studies are important and provide an academic reference for further studying the mechanical behavior of QCs.

In engineering applications, various defects such as dislocation, crack, and inclusion will have an adverse impact on the performance of QC materials. Thus, it is very important to investigate the influences of defects on mechanical behaviors for QCs. Fan et al. [14] studied one-dimensional (1D) hexagonal QC with a linear crack in a thermoelastic framework by the extended displacement discontinuity method. Guo et al. [15] explored the III-mode crack in a 1D hexagonal QC strip and obtained the explicit expressions of generalized stress intensity factors around the crack tip. Zhou and Li [16] considered the mechanics characteristic of 1D piezoelectric quasicrystals (PQCs) with anti-plane Yoffe-type moving cracks. Li et al. [17] analyzed the mutual effect between a spiral dislocation and an elliptic hole containing two unsymmetrical cracks in a 1D hexagonal piezoelectric QC and obtained the analytical expressions of image force. Recently, Mu et al. [18] researched the planar problem of functionally graded two-dimensional (2D) PQC wedges and spaces and carefully discussed the effects of line force, charge, and dislocation on electric potential and stresses. These theories can serve as benchmarks for further research on QCs.

As we all know, the Green's function is one of the most powerful tools to investigate planar problems. Whereas, Green's function for QCs is rather complicated due to the coupling of phonon and phason. In recent years, Zhang et al. [19] obtained Green's functions of displacements and stresses for 1D PQC bi-material with multi-physics loadings by the Stroh formalism. Wu et al. [20] explored 1D PQC semi-infinite plane and infinite plane under different loading conditions, utilizing the same method. Later on, Xu et al. [21] extended Ref. [14] to 2D PQC and studied the influences of line force and dislocation on the mechanical behaviors of QC in detail. Gao and Ricoeur [22] presented 3D Green's function of infinite 2D QC bi-material. Wang [23] obtained the time-harmonic dynamic Green's functions of 1D hexagonal QCs with line forces along the quasiperiodic axis and analyzed the asymptotic behaviors of the Green's function in the far field. Li and Li [24] obtained the explicit expressions of Eshelby tensors for some special cases, such as elliptic cylinder and spheroid, for 1D hexagonal QCs through Green's function method. These researches are beneficial for us to pursue the complicated properties of QCs further.

Stroh formalism is a powerful and elegant method for 2D deformation problems [25–27], assuming that displacement depends on x and y only. Ting [28] has successfully shown symmetrical expressions of stress and strain in the Stroh formalism and obtained fundamental solutions for anisotropic wedges [29–32]. In this paper, the Stroh formalism is used to research the image force and mechanical behaviors of cubic PQC semi-infinite space and bi-material composite space under multi-physical loading conditions. At the same time, the explicit expressions of Green's functions for generalized displacement and stress are obtained, and the explicit form of image force in terms of generalized line dislocation is deduced. Some results of numerical examples are given to show the distribution of image force and the coupling behaviors of PQC.

2 The Stroh formalism

QCs possess phonon field and phason field that differs from crystals [33]. The phonon field depicts lattice waves caused by small oscillations of atoms away from the equilibrium, similar to that found in usual crystals. The phason field stands for the rearrangement or flip of atoms in the real structure [34]. The cubic QCs mean that atomic arrangements exhibit quasiperiodicity in each direction (x_1, x_2, and x_3). In the recent literature, several studies have been conducted on cubic QCs. Long and Li [35, 36] paid attention to the Flamant problem of a cubic QC half-plane and obtained the closed-form solution for a rotating cubic QC disk. In addition, they derived a thermoelastic solution for a circular disk by the semi-inversion method [37]. Mu et al. [38] analyzed

the singularities of cubic PQC composite wedges and spaces. It can be found that the planar problems of cubic QCs have been studied to some extent, but not far enough. Thus, the image force of cubic QCs with piezoelectric effect is worthwhile for further research.

On the basis of QC elastic theory [34], the basic equations of cubic PQCs polarized along the x_3-direction with point group $\bar{4}3$ m are expressible as follows:

$$\varepsilon_{ij} = \frac{1}{2}\left(\frac{\partial u_i}{\partial x_j} + \frac{\partial u_j}{\partial x_i}\right),\ w_{ij} = \frac{1}{2}\left(\frac{\partial w_i}{\partial x_j} + \frac{\partial w_j}{\partial x_i}\right),\ E_i = -\frac{\partial \phi}{\partial x_i}, \tag{1}$$

$$\begin{aligned}
\sigma_{11} &= C_{11}\varepsilon_{11} + C_{12}\varepsilon_{22} + C_{12}\varepsilon_{33} + R_1 w_{11} + R_2 w_{22} + R_2 w_{33},\\
\sigma_{22} &= C_{12}\varepsilon_{11} + C_{11}\varepsilon_{22} + C_{12}\varepsilon_{33} + R_2 w_{11} + R_1 w_{22} + R_2 w_{33},\\
\sigma_{33} &= C_{12}\varepsilon_{11} + C_{12}\varepsilon_{22} + C_{11}\varepsilon_{33} + R_2 w_{11} + R_2 w_{22} + R_1 w_{33},\\
\sigma_{23} &= \sigma_{32} = 2C_{44}\varepsilon_{23} + 2R_3 w_{23} - d_{14}E_1,\\
\sigma_{31} &= \sigma_{13} = 2C_{44}\varepsilon_{31} + 2R_3 w_{31} - d_{14}E_2,\\
\sigma_{12} &= \sigma_{21} = 2C_{44}\varepsilon_{12} + 2R_3 w_{12} - d_{14}E_3,
\end{aligned} \tag{2}$$

$$\begin{aligned}
H_{11} &= R_1\varepsilon_{11} + R_2\varepsilon_{22} + R_2\varepsilon_{33} + K_{11}w_{11} + K_{12}w_{22} + K_{12}w_{33},\\
H_{22} &= R_2\varepsilon_{11} + R_1\varepsilon_{22} + R_2\varepsilon_{33} + K_{12}w_{11} + K_{11}w_{22} + K_{12}w_{33},\\
H_{33} &= R_2\varepsilon_{11} + R_2\varepsilon_{22} + R_1\varepsilon_{33} + K_{12}w_{11} + K_{12}w_{22} + K_{11}w_{33},\\
H_{23} &= H_{32} = 2R_3\varepsilon_{23} + 2K_{44}w_{23} - d_{123}E_1,\\
H_{31} &= H_{13} = 2R_3\varepsilon_{31} + 2K_{44}w_{31} - d_{123}E_2,\\
H_{12} &= H_{21} = 2R_3\varepsilon_{12} + 2K_{44}w_{12} - d_{123}E_3,\\
D_1 &= 2d_{14}\varepsilon_{23} + 2d_{123}w_{23} + \xi_{11}E_1,\\
D_2 &= 2d_{14}\varepsilon_{31} + 2d_{123}w_{31} + \xi_{22}E_2,\\
D_3 &= 2d_{14}\varepsilon_{12} + 2d_{123}w_{12} + \xi_{33}E_3,
\end{aligned} \tag{3}$$

$$\partial_j\sigma_{ij} = 0,\ \partial_j H_{ij} = 0,\ \partial_j D_j = 0.$$

where $i,\ j = 1,\ 2,\ 3$, u_i and w_i represent the displacement components in the phonon and phason fields, respectively; ε_{ij} and σ_{ij} are strain and stress components in the phonon field, respectively; w_{ij} and H_{ij} are strain and stress components in the phason field, respectively; E_i, ϕ, and D_j denote electric field intensities, electric potential, and electric displacements, respectively; C_{ij} and K_{ij} are the elastic constants in the phonon and phason fields, respectively; R_i are the phonon–phason coupled elastic constants; d_{14} and d_{123} are the piezoelectric constants in the phonon and phason fields, respectively; and ξ_{ij} are the dielectric constants.

When a straight dislocation or a Griffith crack exists along the direction of the atom quasiperiodic arrangement, a 3D problem can be considered as a 2D deformation problem. For 2D deformation, the displacement fields are assumed as dependent on the x_1 and x_3, and independent of x_2. Therefore, the general solution of displacement meeting Eqs. (1), (2), and (3) is expressed as follows:

$$\mathbf{u} = \mathbf{a}f(z),\ z = x_1 + px_3, \tag{4}$$

where

$$\mathbf{u} = [u_1, u_2, u_3, w_1, w_2, w_3, \phi]^T, \tag{5}$$

$\mathbf{a}$ and p are the material eigenvectors and eigenvalues, f is an arbitrary function of z, and the superscript "T" denotes matrix transpose.

By virtue of Eqs. (1), (2), (3), and (4), we have

$$\left[\mathbf{Q} + p\left(\mathbf{R} + \mathbf{R}^T\right) + p^2\mathbf{T}\right]\mathbf{a} = \mathbf{0}, \tag{6}$$

where $\mathbf{Q}$, $\mathbf{R}$, and $\mathbf{T}$ are 7×7 real matrices associated with material constants, which can be denoted by Eq. (A1) in the Appendix.

With the aid of Eqs. (2), (4), and (6), the generalized stress function $\boldsymbol{\varphi}$ has the following form

$$\boldsymbol{\varphi} = \mathbf{b}f(z). \tag{7}$$

$\mathbf{b}$ is a vector associated with $\mathbf{a}$ and obtained by Eq. (6).

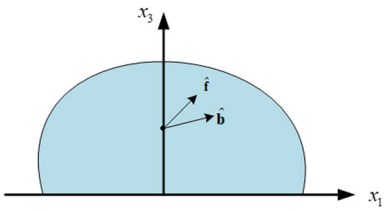

Fig. 1 Generalized line force $\hat{\mathbf{f}}$ and dislocation $\hat{\mathbf{b}}$ co-exist at the point $(0, d)$

We have [39]

$$\mathbf{N}\begin{bmatrix}\mathbf{a}\\ \mathbf{b}\end{bmatrix} = p\begin{bmatrix}\mathbf{a}\\ \mathbf{b}\end{bmatrix}, \tag{8}$$

$$\mathbf{N} = \begin{bmatrix}\mathbf{N}_1 & \mathbf{N}_2\\ \mathbf{N}_3 & \mathbf{N}_1^T\end{bmatrix}, \mathbf{N}_1 = -\mathbf{T}^{-1}\mathbf{R}^T, \mathbf{N}_2 = \mathrm{T}^{-1}, \mathbf{N}_3 = \mathbf{R}\mathbf{T}^{-1}\mathbf{R}^T - \mathbf{Q}, \tag{9}$$

where

$$\begin{aligned} &p_{\alpha+7} = \overline{p}_\alpha,\ \mathrm{Im}p_\alpha > 0,\\ &\mathbf{a}_{\alpha+7} = \overline{\mathbf{a}}_\alpha,\ \mathbf{b}_{\alpha+7} = \overline{\mathbf{b}}_\alpha,\ (\alpha = 1, 2, ..., 7). \end{aligned} \tag{10}$$

"Im" and overbar represent the imaginary part and complex conjugate, respectively.
$\mathbf{u}$ and $\boldsymbol{\varphi}$ can be rewritten as [3],

$$\mathbf{u} = \mathrm{Im}\big[\mathbf{A} < \mathbf{f}(z_\alpha) > \mathbf{q}\big],\ \boldsymbol{\varphi} = \mathrm{Im}\big[\mathbf{B} < \mathbf{f}(z_\alpha) > \mathbf{q}\big],\ z_\alpha = x_1 + p_\alpha x_3, \tag{11}$$

in which

$$\begin{aligned} &\mathbf{A} = [\mathbf{a}_1, \mathbf{a}_2, \mathbf{a}_3, \mathbf{a}_4, \mathbf{a}_5, \mathbf{a}_6, \mathbf{a}_7],\ \mathbf{B} = [\mathbf{b}_1, \mathbf{b}_2, \mathbf{b}_3, \mathbf{b}_4, \mathbf{b}_5, \mathbf{b}_6, \mathbf{b}_7],\\ &\mathbf{f}(z_\alpha) = [f_1(z_1), f_2(z_2), f_3(z_3), f_4(z_4), f_5(z_5), f_6(z_6), f_7(z_7)]^T, \end{aligned} \tag{12}$$

and "$<>$" denotes diagonal matrix. $\mathbf{A}$ and $\mathbf{B}$ have the orthogonal relation

$$\begin{aligned} &\mathbf{B}^T\mathbf{A} + \mathbf{A}^T\mathbf{B} = \mathbf{I} = \overline{\mathbf{B}}^T\overline{\mathbf{A}} + \overline{\mathbf{A}}^T\overline{\mathbf{B}},\\ &\mathbf{B}^T\overline{\mathbf{A}} + \mathbf{A}^T\overline{\mathbf{B}} = \mathbf{0} = \overline{\mathbf{B}}^T\mathbf{A} + \overline{\mathbf{A}}^T\mathbf{B}. \end{aligned} \tag{13}$$

Barnett–Lothe matrices $\mathbf{S}$, $\mathbf{H}$, and $\mathbf{L}$ are introduced

$$\mathbf{S} = \mathrm{i}\left(2\mathbf{A}\mathbf{B}^T - \mathbf{I}\right),\ \mathbf{H} = 2\mathrm{i}\mathbf{A}\mathbf{A}^T,\ \mathbf{L} = -2\mathrm{i}\mathbf{B}\mathbf{B}^T, \tag{14}$$

where i is an imaginary number, and I is a 7×7 identity matrix. Moreover, they satisfy the following equation

$$\mathbf{H}\mathbf{L} - \mathbf{S}\mathbf{S} = \mathbf{I}. \tag{15}$$

3 The Green's functions of cubic PQC semi-infinite space

Considering the semi-infinite space of a cubic PQC, phonon line forces $f_i^{\parallel}(i = 1, 2, 3)$, phason line forces $f_j^{\perp}(j = 1, 2, 3)$, line charge λ, phonon line dislocations $b_i^{\parallel}(i = 1, 2, 3)$, phason line dislocations $b_j^{\perp}(j = 1, 2, 3)$, and electric potential jump b^{ϕ} act simultaneously at the point $(0, d)$, $\left(\hat{\mathbf{f}} = \left[f_1^{\parallel}, f_2^{\parallel}, f_3^{\parallel}, f_1^{\perp}, f_2^{\perp}, f_3^{\perp}, -\lambda\right]^T,\ \hat{\mathbf{b}} = \left[b_1^{\parallel}, b_2^{\parallel}, b_3^{\parallel}, b_1^{\perp}, b_2^{\perp}, b_3^{\perp}, b^{\phi}\right]^T\right)$, as depicted in Fig. 1.

$$(x_1, x_3) = (0, d), \tag{16}$$

Take the form $\mathbf{f}(z_\alpha)$ as $< \ln z_\alpha >$ and insert it into Eq. (11) to obtain [3]

$$\begin{aligned}\mathbf{u} &= \frac{1}{\pi}\mathrm{Im}\big[\mathbf{A} < \ln(z_\alpha - p_\alpha d) > \mathbf{q}\big] + \frac{1}{\pi}\mathrm{Im}\sum_{\beta=1}^{7}\big[\mathbf{A} < \ln\big(z_\alpha - \overline{p}_\beta d\big) > \mathbf{q}_\beta\big],\\ \boldsymbol{\varphi} &= \frac{1}{\pi}\mathrm{Im}\big[\mathbf{B} < \ln(z_\alpha - p_\alpha d) > \mathbf{q}\big] + \frac{1}{\pi}\mathrm{Im}\sum_{\beta=1}^{7}\big[\mathbf{B} < \ln\big(z_\alpha - \overline{p}_\beta d\big) > \mathbf{q}_\beta\big],\end{aligned} \tag{17}$$

where

$$\mathbf{q} = \mathbf{A}^T\hat{\mathbf{f}} + \mathbf{B}^T\hat{\mathbf{b}}, \tag{18}$$

and

$$< \ln\big(z_\alpha - \overline{p}_\beta d\big) >= \mathrm{diag}\big[\ln\big(z_1 - \overline{p}_\beta d\big),\ \ln\big(z_2 - \overline{p}_\beta d\big),\ ...,\ \ln\big(z_7 - \overline{p}_\beta d\big)\big].$$

In the above, $\mathbf{q}_\beta$ are unknown complex coefficient vectors to be settled. The first terms of Eq. (17) denote Green's function for an infinite space with multiple loadings applied at the location shown by Eq. (16). The second terms about sum in Eq. (17) are the disturbed solutions satisfying the boundary condition at $x_3 = 0$.

Suppose that the surface $x_3 = 0$ is traction-free and electrically open, namely,

$$\boldsymbol{\varphi} = \mathbf{0},\ \text{at}\ x_3 = 0. \tag{19}$$

Substituting Eq. $(17)_2$ into Eq. (19) gets an alternative expression

$$\mathrm{Im}\big[\mathbf{B} < \ln(x_1 - p_\alpha d) > \mathbf{q}\big] + \mathrm{Im}\sum_{\beta=1}^{7}\big[\ln\big(x_1 - \overline{p}_\beta d\big)\mathbf{B}\mathbf{q}_\beta\big] = \mathbf{0}, \tag{20}$$

the first term can be replaced by the negative of its complex conjugate, to wit

$$\mathrm{Im}\big[\mathbf{B} < \ln(x_1 - p_\alpha d) > \mathbf{q}\big] = -\mathrm{Im}\big[\overline{\mathbf{B}} < \ln\big(x_1 - \overline{p}_\alpha d\big) > \overline{\mathbf{q}}\big], \tag{21}$$

where

$$\begin{aligned}< \ln\big(x_1 - \overline{p}_\alpha d\big) >&= \sum_{\beta=1}^{7}\big[\ln\big(x_1 - \overline{p}_\beta d\big)\mathbf{I}_\beta\big],\\ \mathbf{I}_\beta &= \mathrm{diag}\big[\delta_{\beta1}, \delta_{\beta2}, \delta_{\beta3}, \delta_{\beta4}, \delta_{\beta5}, \delta_{\beta6}, \delta_{\beta7}\big],\end{aligned} \tag{22}$$

where $\delta_{\beta i}$ are the Kronecker's delta.

By Eqs. (21) and (22), Eq. (20) is simplified as

$$\mathbf{B}\mathbf{q}_\beta = \overline{\mathbf{B}}\mathbf{I}_\beta\overline{\mathbf{q}}, \tag{23}$$

which obtains

$$\mathbf{q}_\beta = \mathbf{B}^{-1}\overline{\mathbf{B}}\mathbf{I}_\beta\overline{\mathbf{q}}. \tag{24}$$

Assume that the surface $x_3 = 0$ is clamped and electrically closed, i.e.,

$$\mathbf{u} = \mathbf{0},\ \text{at}\ x_3 = 0. \tag{25}$$

Due to the similarity, we derive

$$\mathbf{q}_\beta = \mathbf{A}^{-1}\overline{\mathbf{A}}\mathbf{I}_\beta\overline{\mathbf{q}}. \tag{26}$$

Ref. [3] provided the foundations of the present study and attached importance to the anisotropic elastic material, while our work conducted the cubic PQC. It is more complicated because of the coupling effect of the phonon, phason, and electric fields. Since mathematical expressions of the Stroh formalism are simple and compact, the method and formulation can be easily extended to other materials, such as 1D and 2D QCs.

4 Image force for semi-infinite space

The image force F induced by the line dislocation and the boundary $x_3 = 0$ is [40]

$$F = -\sigma_{i1}^{d} b_i = \mathbf{b}^T \boldsymbol{\varphi}_{,3}^{d}, \tag{27}$$

where σ_{i1}^{d} is the stress derived from the second term in Eq. $(17)_2$ at the point $(0, d)$.

With the aid of Eq. (22), we have

$$\begin{aligned} F &= \frac{1}{\pi d}\mathrm{Im}\sum_{\beta=1}^{7}\mathbf{b}^T\left[\mathbf{B} < \frac{p_\alpha}{p_\alpha - \overline{p}_\beta} > \mathbf{q}_\beta\right] \\ &= \frac{1}{\pi d}\mathrm{Im}\sum_{\beta=1}^{7}\sum_{\alpha=1}^{7}\mathbf{b}^T\left[\frac{p_\alpha}{p_\alpha - \overline{p}_\beta}\mathbf{B}\mathbf{I}_\alpha\mathbf{q}_\beta\right]. \end{aligned} \tag{28}$$

When the boundary is traction-free and electrically open, substituting Eq. (24) with $\mathbf{q} = \mathbf{B}^T\,\mathbf{b}$ into Eq. (28) and using Eq. (14) obtains

$$F=\frac{-1}{2\pi d}\mathrm{Re}\sum_{\beta=1}^{7}\sum_{\alpha=1}^{7}\mathbf{b}^T\left[\frac{p_\alpha}{p_\alpha - \overline{p}_\beta}\left(\mathbf{B}\mathbf{I}_\alpha\mathbf{B}^{-1}\right)\mathbf{L}\left(\overline{\mathbf{B}}\mathbf{I}_\beta\overline{\mathbf{B}}^{-1}\right)^T\right]\mathbf{b}. \tag{29}$$

We have

$$F=\frac{-1}{2\pi d}\mathrm{Re}\sum_{\beta=1}^{7}\sum_{\alpha=1}^{7}\mathbf{b}^T\left[\frac{-\overline{p}_\beta}{p_\alpha - \overline{p}_\beta}\left(\mathbf{B}\mathbf{I}_\alpha\mathbf{B}^{-1}\right)\mathbf{L}\left(\overline{\mathbf{B}}\mathbf{I}_\beta\overline{\mathbf{B}}^{-1}\right)^T\right]\mathbf{b}, \tag{30}$$

the above derivation process is shown in Eqs. (A2) and (A3) in the Appendix.

Equation (29) is superposed on Eq. (30) to yield

$$F=\frac{-1}{4\pi d}\mathrm{Re}\sum_{\beta=1}^{7}\sum_{\alpha=1}^{7}\mathbf{b}^T\left[\left(\mathbf{B}\mathbf{I}_\alpha\mathbf{B}^{-1}\right)\mathbf{L}\left(\overline{\mathbf{B}}\mathbf{I}_\beta\overline{\mathbf{B}}^{-1}\right)^T\right]\mathbf{b}, \tag{31}$$

Equation (31) is reduced to

$$F=\frac{-1}{4\pi d}\mathbf{b}^T\mathbf{L}\mathbf{b}, \tag{32}$$

Equation (32) refers to the image force caused by the traction-free and electrically open surface, which can be downgraded to the solution of image force caused by crack [41] by replacing the coefficient 1/4 to 1/8. Owing to the positive definiteness of $\mathbf{L}$, $F < 0$, the image force always attracts the dislocation to the boundary.

When the boundary is fixed, substitution of Eq. (26) into Eq. (28) and using Eq. (14) yields

$$F=\frac{1}{2\pi d}\mathrm{Re}\sum_{\beta=1}^{7}\sum_{\alpha=1}^{7}\mathbf{b}^T\left[\frac{p_\alpha}{p_\alpha - \overline{p}_\beta}\left(\mathbf{B}\mathbf{I}_\alpha\mathbf{A}^{-1}\right)\mathbf{H}\left(\overline{\mathbf{B}}\mathbf{I}_\beta\overline{\mathbf{A}}^{-1}\right)^T\right]\mathbf{b}. \tag{33}$$

Following the similar operation of Eqs. (30) and (31), we have

$$F=\frac{1}{4\pi d}\mathbf{b}^T\left[\mathbf{H}^{-1} - \mathbf{H}^{-1}\mathbf{S}\mathbf{S}\right]\mathbf{b}, \tag{34}$$

by means of Eq. (15), we get

$$F=\frac{1}{4\pi d}\mathbf{b}^T\left(2\mathbf{H}^{-1} - \mathbf{L}\right)\mathbf{b}. \tag{35}$$

With the help of Eqs. (A4) and (A5) in the Appendix, we can draw the conclusion that $F > 0$. This means that the image force always rejects the dislocation to the boundary.

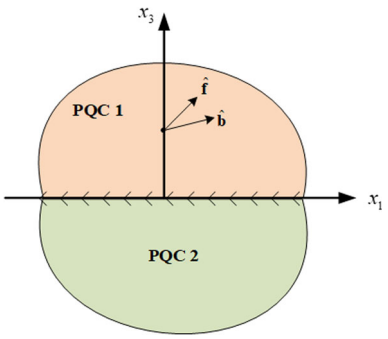

Fig. 2 Generalized line force $\hat{\mathbf{f}}$ and dislocation $\hat{\mathbf{b}}$ are applied to the point $(0, d)$ in the composite infinite space

5 Image force for bi-material composite space

Considering a composite infinite space contains two dissimilar cubic PQC half-spaces. Generalized line force and dislocation are applied to the point given by Eq. (16) as shown in Fig. 2.

Due to displacements and stresses continuity along the interface, we have

$$\mathbf{u}_1 = \mathbf{u}_2,\ \boldsymbol{\varphi}_1 = \boldsymbol{\varphi}_2,\ \text{at } x_3 = 0, \tag{36}$$

for material 1, Eq. (17) can be rewritten as

$$\begin{aligned}
\mathbf{u}_1 &= \frac{1}{\pi}\mathrm{Im}\left[\mathbf{A}_1 < \ln\left(z_\alpha^{(1)} - p_\alpha^{(1)} d\right) > \mathbf{q}\right] + \frac{1}{\pi}\mathrm{Im}\sum_{\beta=1}^{7}\left[\mathbf{A}_1 < \ln\left(z_\alpha^{(1)} - \overline{p}_\beta^{(1)} d\right) > \mathbf{q}_\beta^{(1)}\right], \\
\boldsymbol{\varphi}_1 &= \frac{1}{\pi}\mathrm{Im}\left[\mathbf{B}_1 < \ln\left(z_\alpha^{(1)} - p_\alpha^{(1)} d\right) > \mathbf{q}\right] + \frac{1}{\pi}\mathrm{Im}\sum_{\beta=1}^{7}\left[\mathbf{B}_1 < \ln\left(z_\alpha^{(1)} - \overline{p}_\beta^{(1)} d\right) > \mathbf{q}_\beta^{(1)}\right],
\end{aligned} \tag{37}$$

for material 2,

$$\begin{aligned}
\mathbf{u}_2 &= \frac{1}{\pi}\mathrm{Im}\sum_{\beta=1}^{7}\left[\mathbf{A}_2 < \ln\left(z_\alpha^{(2)} - p_\beta^{(1)} d\right) > \mathbf{q}_\beta^{(2)}\right], \\
\boldsymbol{\varphi}_2 &= \frac{1}{\pi}\mathrm{Im}\sum_{\beta=1}^{7}\left[\mathbf{B}_2 < \ln\left(z_\alpha^{(2)} - p_\beta^{(1)} d\right) > \mathbf{q}_\beta^{(2)}\right].
\end{aligned} \tag{38}$$

In the above, all quantities with subscripts 1 and 2 or the superscripts (1) and (2) correspond to material 1 and material 2, respectively. $\mathbf{q}_\beta^{(1)}$ and $\mathbf{q}_\beta^{(2)}$ are unknown constants to be determined.

We have

$$\begin{aligned}
\overline{\mathbf{B}}_2\overline{\mathbf{q}}_\beta^{(2)} &= 2\left(\mathbf{M}_1^{-1} + \overline{\mathbf{M}}_2^{-1}\right)^{-1}\mathbf{L}_1^{-1}\overline{\mathbf{B}}_1\mathbf{I}_\beta\overline{\mathbf{q}}, \\
\mathbf{B}_1\mathbf{q}_\beta^{(1)} &= \left[\mathbf{I} - 2\left(\mathbf{M}_1^{-1} + \overline{\mathbf{M}}_2^{-1}\right)^{-1}\mathbf{L}_1^{-1}\right]\overline{\mathbf{B}}_1\mathbf{I}_\beta\overline{\mathbf{q}}.
\end{aligned} \tag{39}$$

The derivation process of Eq. (39) is shown in Eqs. (A6)–(A14) in the Appendix.

Using Eq. $(39)_2$, the image force can be derived

$$\begin{aligned}
F &= \frac{1}{\pi d}\mathrm{Im}\sum_{\beta=1}^{7}\sum_{\alpha=1}^{7}\mathbf{b}^T\left[\frac{p_\alpha^{(1)}}{p_\alpha^{(1)} - \overline{p}_\beta^{(1)}}\mathbf{B}_1\mathbf{I}_\alpha\mathbf{q}_\beta^{(1)}\right] \\
&= \frac{-1}{4\pi d}\mathbf{b}^T\left[\mathbf{L}_1 - 2\hat{\mathbf{D}}\right]\mathbf{b},
\end{aligned} \tag{40}$$

Table 1 Material constants of the cubic PQC

Material constants	PQC 1	PQC 2
Phonon field (GPa)	$C_{11} = 166, C_{12} = 77,$ $C_{44} = 88$	$C_{11} = 286, C_{12} = 173,$ $C_{44} = 170.5$
Phason field (GPa)	$K_{11} = 24,\ K_{12} = 14,\ K_{44} = 19$	$K_{11} = 145,\ K_{12} = 57,\ K_{44} = 33$
Couple field (GPa)	$R_1 = 8.85,\ R_2 = 4.85,\ R_3 = 5.85$	$R_1 = 13.7,\ R_2 = 7.5,\ R_3 = 10.4$
Piezoelectric constant $\left(\mathrm{Cm}^{-2}\right)$	$d_{14} = -0.138, d_{123} = -0.16$	$d_{14} = -0.247, d_{123} = -0.2674$
Dielectric constants $\left(10^{-9}\ \mathrm{C}^2/(\mathrm{Nm}^2)\right)$	$k_1 = 11.2, k_2 = 8.2,\ k_3 = 4.2$	$k_1 = 22.4, k_2 = 14.3,\ k_3 = 6.9$

where

$$\hat{\mathbf{D}}=\left[\mathbf{L}_1^{-1}+\mathbf{L}_2^{-1}+\left(\mathbf{S}_1\mathbf{L}_1^{-1}-\mathbf{S}_2\mathbf{L}_2^{-1}\right)\left(\mathbf{L}_1^{-1}+\mathbf{L}_2^{-1}\right)^{-1}\left(\mathbf{S}_1\mathbf{L}_1^{-1}-\mathbf{S}_2\mathbf{L}_2^{-1}\right)\right]^{-1} \tag{41}$$

One point worth emphasizing that the solutions of generalized displacement and stress depend upon x_1 and x_3 for the whole theoretical deduction. Owing to the similarity, the solutions for x_1 and x_2 can be readily acquired.

6 Numerical examples and discussion

Although the preparation technology of QCs has made great progress, the material constants of the cubic QCs with the point group $\overline{4}3$ m have not been fully obtained due to the difficulty of the experiment. From the works of Wang et al. [33] and Fan [34], the physical parameters of cubic PQC satisfy the following properties of symmetry and positive definite

$$\begin{aligned} &C_{ijkl} = C_{jikl} = C_{klij}{=}C_{ijlk},\ K_{ijkl} = K_{klij},\ R_{ijkl} = R_{jikl},\ e_{lij}{=}e_{lji},\ \xi_{jl} = \xi_{lj},\ C_{ijkl}\varepsilon_{ij}\varepsilon_{kl} > 0,\\ &K_{ijkl}w_{ij}w_{kl} > 0,\ \xi_{jl}E_jE_l > 0. \end{aligned} \tag{42}$$

Based on the positive definite conditions, the material constants of cubic PQC can be assumed as follows (Table 1):

To conduct the numerical calculation, the dimensionless method below is employed to keep all the values in the matrix stay in the same order so that to eliminate the matrix singularity, where "l" is the unit length.

$$\begin{aligned} &x_1^* = x_1/l,\ x_3^* = x_3/l,\ u_i^* = u_i/l,\ w_i^* = R_1w_i/(C_{11}l),\\ &\sigma_{ij}^* = \sigma_{ij}/C_{11},\ H_{ij}^* = H_{ij}/R_1,\ D_j^* = D_j/d_{14},\ \phi^* = d_{14}\phi/(C_{11}l), \end{aligned} \tag{43}$$

Case 1 The generalized line force $\hat{\mathbf{f}} = [1,\ 0,\ 0,\ 0,\ 0,\ 0,\ 0]^T$ and dislocation $\hat{\mathbf{b}} = [0,\ 1,\ 0,\ 0,\ 0,\ 0,\ 0]^T$ co-exist at the point (0, 2) in a semi-infinite space with a traction-free surface.

Figure 3 displays the distributions of dimensionless phonon displacement u_1^* and phason displacement w_1^* due to a generalized line force $\hat{\mathbf{f}} = [1,\ 0,\ 0,\ 0,\ 0,\ 0,\ 0]^T$ and dislocation $\hat{\mathbf{b}} = [0,\ 1,\ 0,\ 0,\ 0,\ 0,\ 0]^T$. Obviously, the distribution curves of u_1^* and w_1^* are symmetric about the axis $x_1^* = 0$. The absolute values of u_1^* and w_1^* slowly increase away from the loading position. Moreover, u_1^* is several orders of magnitude bigger than w_1^*, which reflects that $\hat{\mathbf{f}} = [1,\ 0,\ 0,\ 0,\ 0,\ 0,\ 0]^T$ and $\hat{\mathbf{b}} = [0,\ 1,\ 0,\ 0,\ 0,\ 0,\ 0]^T$ have a small influence on atomic rearrangement.

The variations of dimensionless phonon stress σ_{11}^* and phason stress H_{32}^* in the rectangular area $\left\{\left(x_1^*,\ x_3^*\right)|-3 \le x_1^* \le 3,\ 0 \le x_3^* \le 3\right\}$ are shown in Fig. 4. The change curves of σ_{11}^* and H_{32}^* are anti-symmetric about the axis $x_1^* = 0$ and exhibit butterfly-shaped patterns. More importantly, a local stress concentration exists at the loading position.

Figure 5a shows that the image forces F_p, F_s, and F_m are induced by generalized line dislocations $\hat{\mathbf{b}} = [1,\ 0,\ 0,\ 0,\ 0,\ 0,\ 0]^T$, $\hat{\mathbf{b}} = [0,\ 0,\ 0,\ 1,\ 0,\ 0,\ 0]^T$, and $\hat{\mathbf{b}} = [1,\ 0,\ 0,\ 1,\ 0,\ 0,\ 0]^T$, while Fig. 5b exhibits image forces F_c, F_e, and F_q caused by $\hat{\mathbf{b}} = [1,\ 0,\ 0,\ 0,\ 0,\ 0,\ 0]^T$ for different materials such as crystal material, piezoelectric material, and PQC material, respectively. In Fig. 5a, the image forces are negative, which means that they always attract the dislocation to the free boundary. That is because the solid is more likely to deform, and the energy of the dislocation will be reduced near the free surface. By comparing the magnitude, the F_p

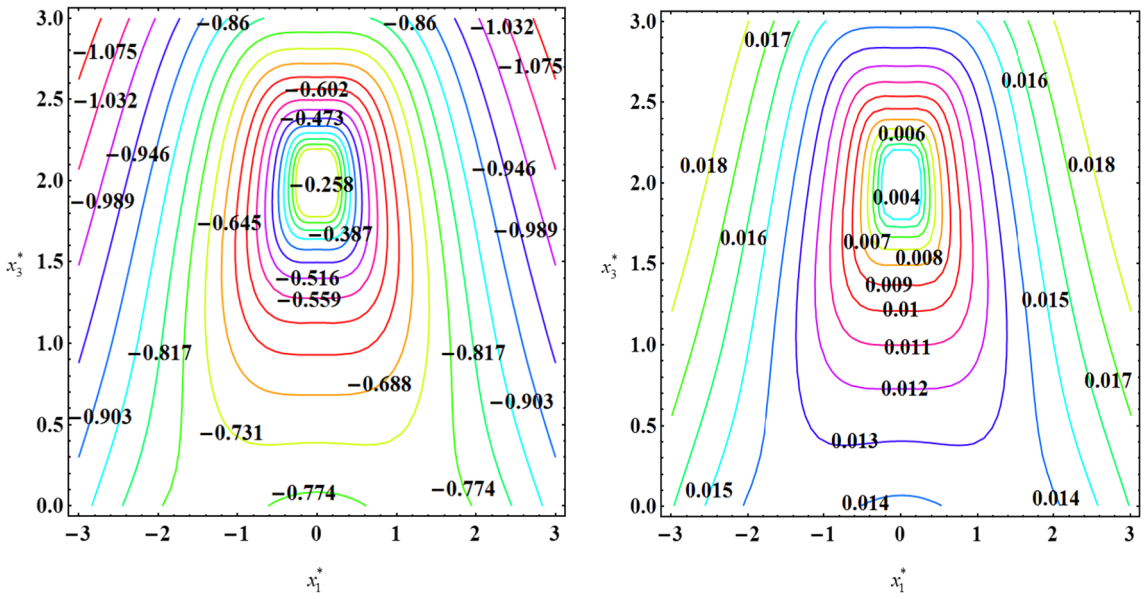

Fig. 3 Distributions of dimensionless phonon and phason displacements: **a** u_1^* and **b** w_1^*

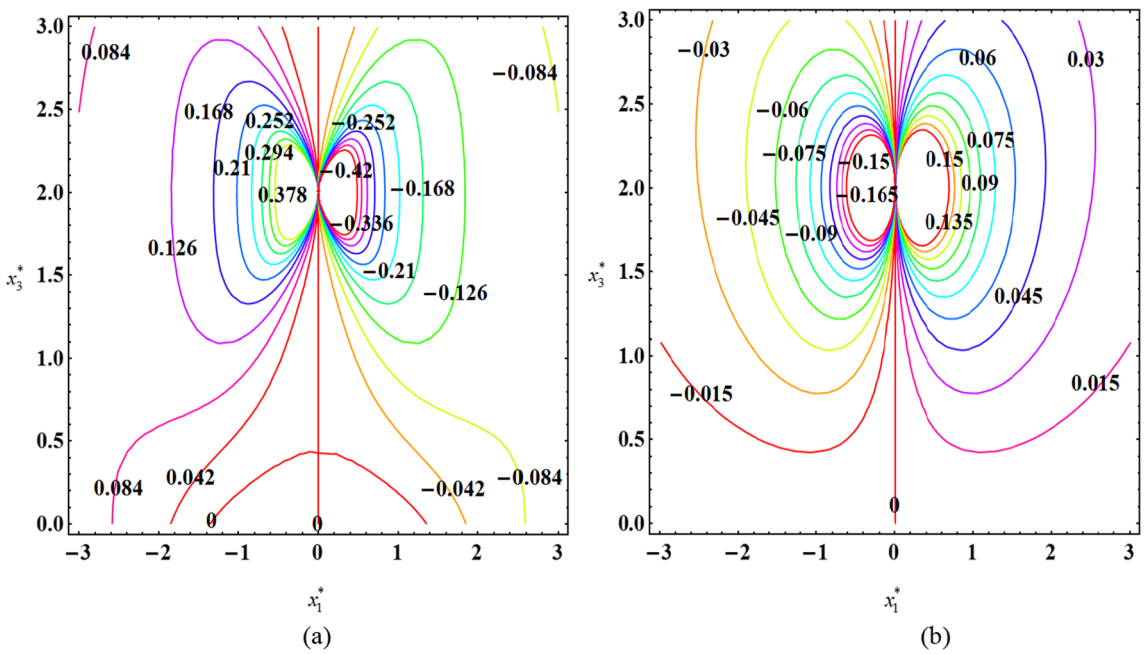

Fig. 4 Distributions of dimensionless phonon and phason stresses: **a** σ_{11}^* and **b** H_{32}^*

is much weaker than F_s and F_m, while F_m is the strongest when phonon and phason dislocations interact together. Moreover, the absolute values of image forces decrease with the increase in d, indicating that the farther the dislocation is from the boundary, the weaker the image force. In Fig. 5b, since there are no evident changes for crystal, piezoelectric material, and PQC, the material properties have little effect on image force under $\hat{\mathbf{b}} = [1, 0, 0, 0, 0, 0, 0]^T$.

Case 2 Both generalized line force $\hat{\mathbf{f}} = [1, 0, 0, 0, 0, 0, 0]^T$ and dislocation $\hat{\mathbf{b}} = [0, 1, 0, 0, 0, 0, 0]^T$ are acting at the point (0, 2) in a semi-infinite space with a fixed surface.

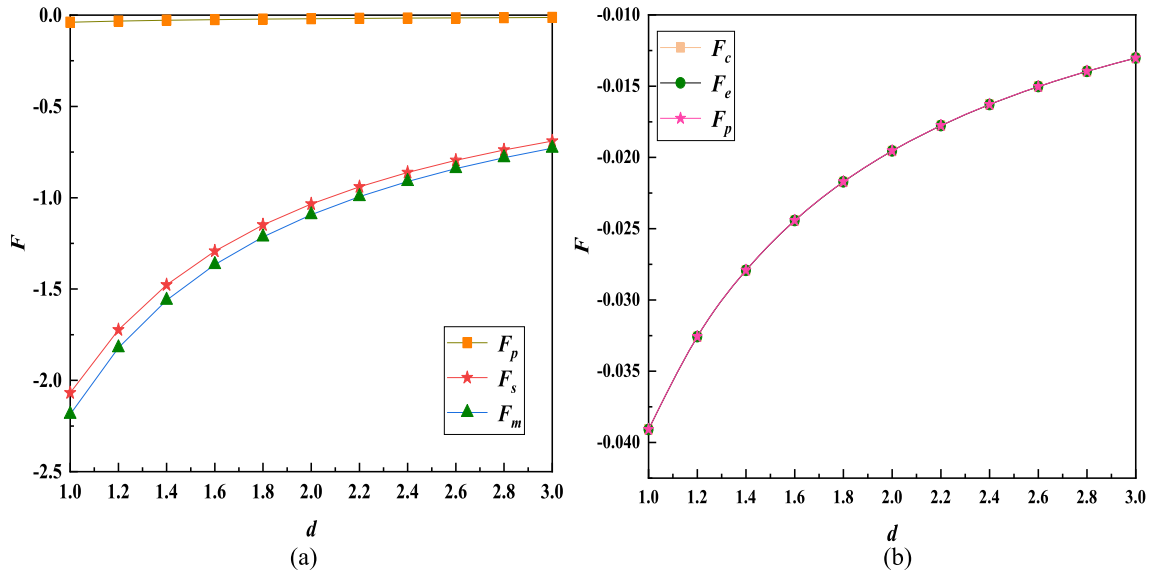

Fig. 5 Image force with a traction-free surface: **a** under different dislocation loadings and **b** for different materials

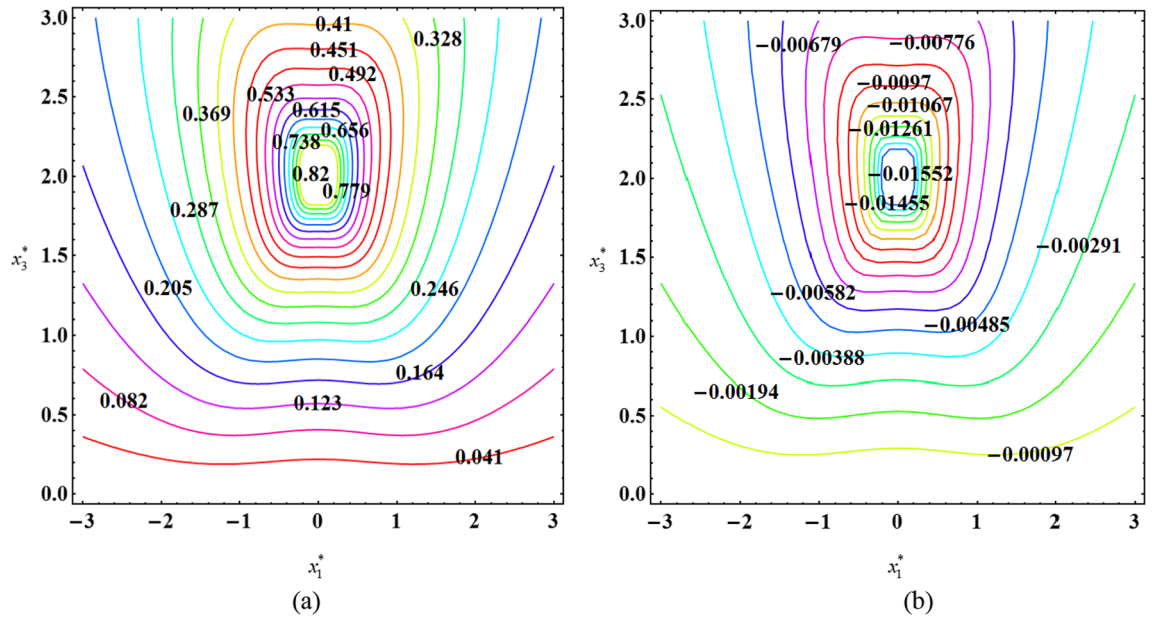

Fig. 6 Variations of dimensionless phonon and phason displacements with a fixed surface: **a** u_1^* and **b** w_1^*

The changes of phonon displacement u_1^* and phason displacement w_1^* are plotted in Fig. 6. Apparently, the symmetries of u_1^* and w_1^* are the same with those in Fig. 3. The displacements which are induced by a generalized line force $\hat{\mathbf{f}} = [1, 0, 0, 0, 0, 0, 0]^T$ and dislocation $\hat{\mathbf{b}} = [0, 1, 0, 0, 0, 0, 0]^T$ increase gradually near the loading position. Remarkably, the shape of the contour in Fig. 6a is analogous to that in Fig. 6b, which reflects the cubic crystallographic symmetry of cubic QC.

Figure 7 shows the contours of dimensionless electric potential ϕ^* and electric displacement D_1^*. ϕ^* is an even function about variable x_1^*, while D_1^* is an odd function concerning x_1^*. The values of ϕ^* approach zero, indicate that line force and line dislocation have negligible effects on electric potential. Moreover, the isopleth map of D_1^* under a single line force shows that the piezoelectric effect of cubic PQC is very evident.

The variations of image forces F_p, F_s, F_m, F_c, F_e, and F_q with d are presented in Fig. 8. Clearly, image forces are greater than zero, namely, image force is easy to push the dislocation away from the boundary $x_3^* = 0$.

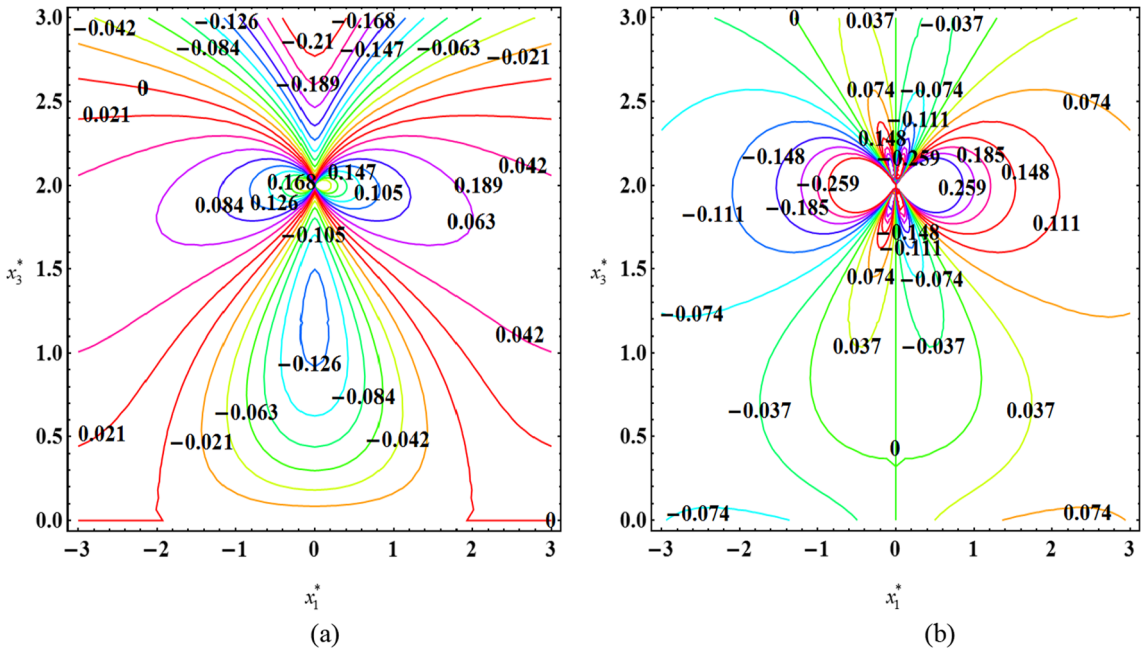

Fig. 7 Contours of dimensionless electric potential and electric displacement: **a** $\phi^*(10^{-5})$ and **b** D_1^*

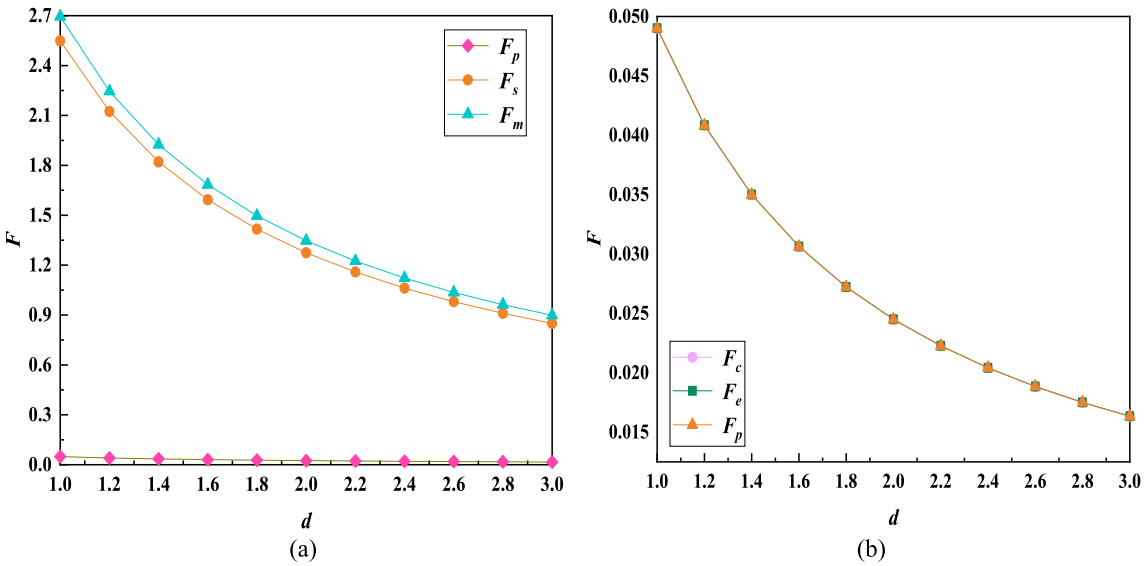

Fig. 8 Image force with a fixed surface: **a** under different dislocation loadings and **b** for different materials

By comparing the magnitudes of graphs, the image force F_m is the greatest under both generalized line force and line dislocation, and image forces F_c, F_e, and F_q have negligible changes for crystal, piezoelectric material, and PQC, which are consistent with Fig. 5.

Case 3 A generalized line force $\hat{\mathbf{f}} = [1, 0, 0, 0, 0, 0, 0]^T$ exists at the point (0, 2) of the bi-material composite space.

The contours of the dimensionless phonon and phason displacements are illustrated in the quadrate area $\{(x_1^*, x_3^*)|-3 \le x_1^* \le 3, -3 \le x_3^* \le 3\}$ are shown in Fig. 9. The contours of u_1^* and w_1^* are symmetric with respect to x_3^* axis, if generalized line force $\hat{\mathbf{f}} = [1, 0, 0, 0, 0, 0, 0]^T$ is applied at the point (0, 2) of the bi-material composite space. Since generalized line force is acting at this point, the displacement distribution

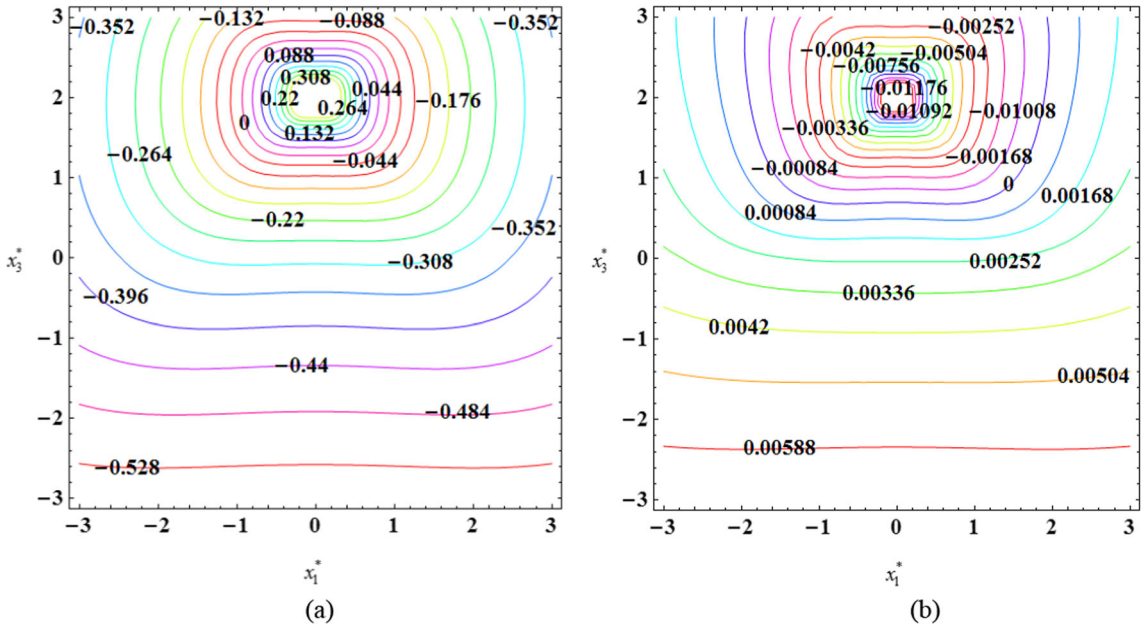

Fig. 9 Variations of dimensionless phonon and phason displacements of infinite space: **a** u_1^* and **b** w_1^*

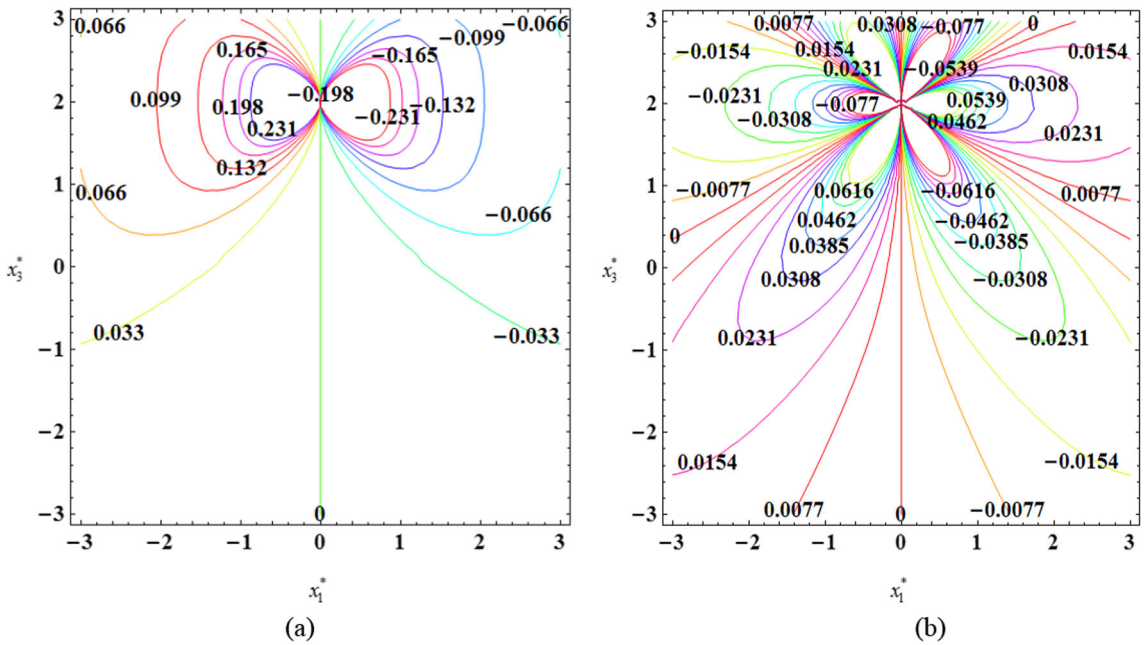

Fig. 10 Variations of dimensionless phonon stresses of infinite space: **a** σ_{11}^* and **b** σ_{33}^*

in the upper half-space is relatively dense, along with local stress concentration. In addition, u_1^* and w_1^* are continuous at the interface to satisfy the boundary condition.

As shown in Fig. 10, the distribution of phonon stresses is antisymmetric with respect to x_3^* axis. The values in the non-polarization direction are slightly larger than those in the polarization direction; thus, the influence of line force on the phonon field along the non-polarization direction is bigger than that along the polarization direction. Another point to note is that the further away from the action point, the less influence the line force has on the phonon field.

Case 4 A line charge $\hat{\mathbf{f}} = [0, 0, 0, 0, 0, 0, 1]^T$ and generalized dislocation $\hat{\mathbf{b}} = [0, 0, 0, 1, 0, 0, 0]^T$ are applied at the point (0, 2) in the composite infinite space.

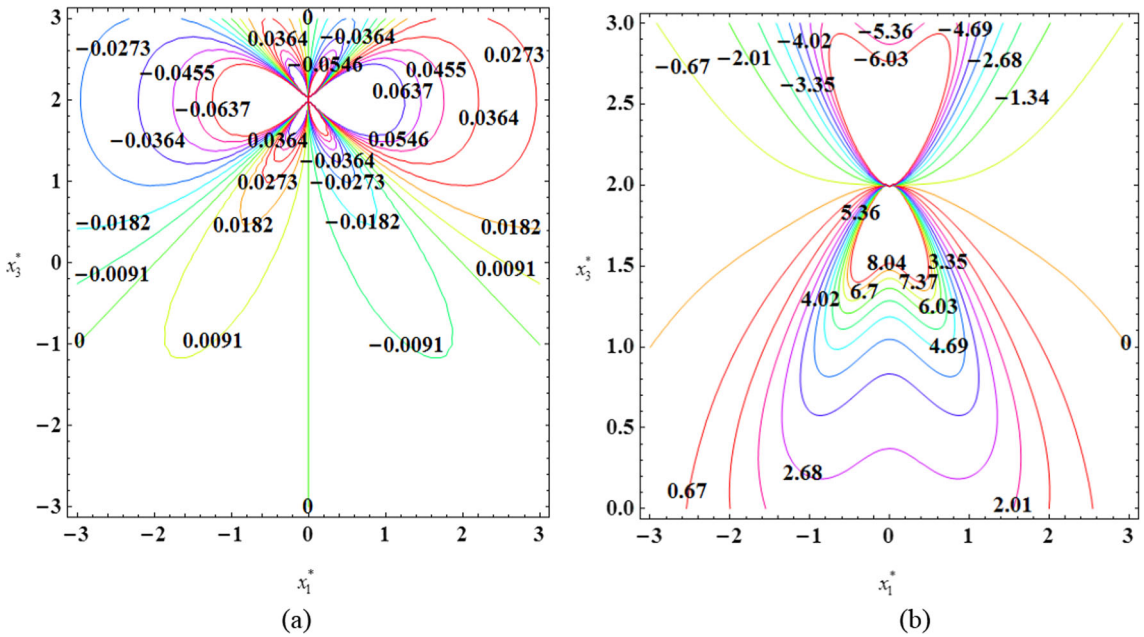

Fig. 11 Variations of dimensionless phonon and phason stresses of infinite space: **a** σ_{13}^{*} and **b** H_{11}^{*}

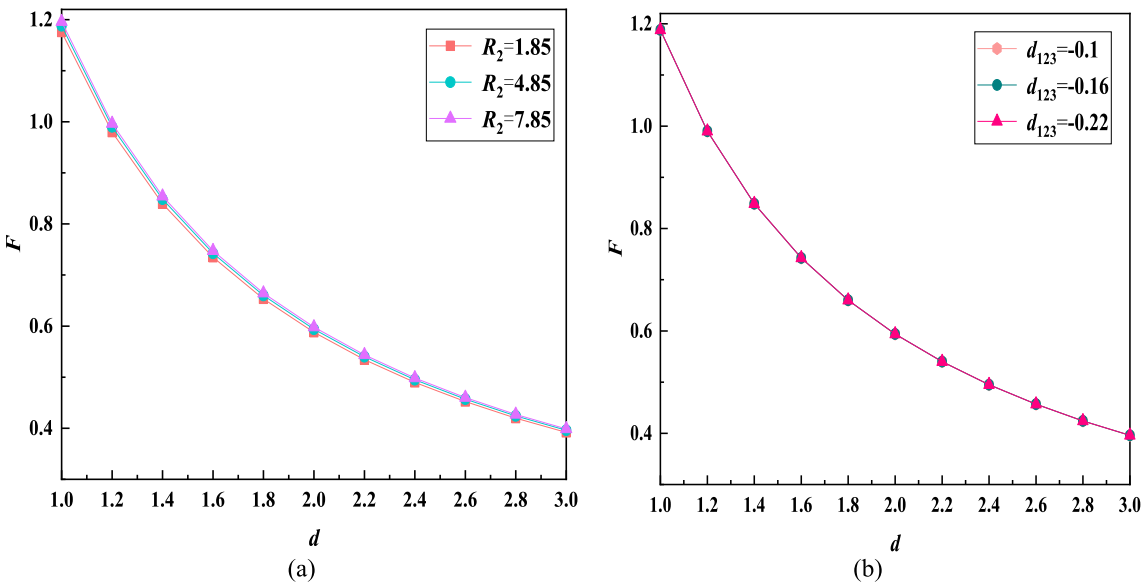

Fig. 12 Variations of image force with: **a** the changes of R_2 and **b** the changes of d_{123}

In Fig. 11, the contours of dimensionless phason stresses H_{11}^{*} are symmetric about x_3^{*} axis. The stresses produced by the line charge reflect the inverse piezoelectric effect. By comparing the magnitude of graphs, the effects of line charge $\hat{\mathbf{f}} = [0, 0, 0, 0, 0, 0, 1]^T$ and generalized dislocation $\hat{\mathbf{b}} = [0, 0, 0, 1, 0, 0, 0]^T$ on phason stress are more obvious than those on phonon stress.

As shown from Fig. 12, the image force F of bi-material composite space is bigger than zero when the upper half-space is subject to a line dislocation $\hat{\mathbf{b}} = [0, 0, 0, 1, 0, 0, 0]^T$, implying that the image force separates the dislocation far from the interface. When the dislocation is closer to the interface, the greater image force is obtained. From Fig. 12, the image force has little effect with phonon–phason coupling constant R_2 and the piezoelectric constant d_{123}.

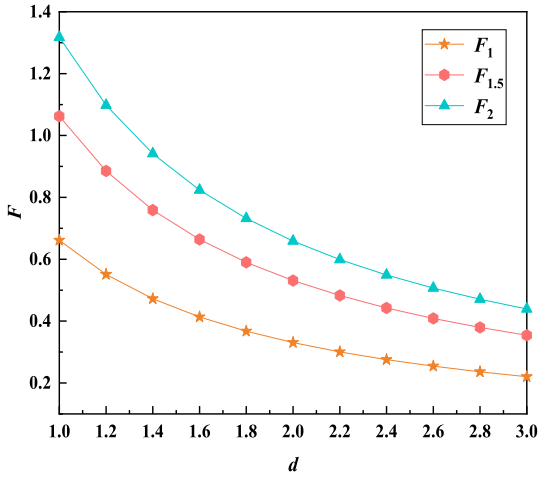

Fig. 13 Variations of image force with different elastic constants of PQC 2

Figure 13 shows the variations of image force F_1, $F_{1.5}$, and F_2 when the elastic constants of PQC 2 are 1 times, 1.5 times, and 2 times of those of PQC 1, respectively. Obviously, the image force enlarges with the increase in elastic constants of PQC 2.

7 Conclusions

Based on the Stroh formalism and Barnett–Lothe matrices, we developed Green's function of displacements and stresses on the 2D deformation problem of cubic PQC semi-infinite space and bi-material composite space under multi-physics loadings. The image forces of semi-infinite space with traction-free or fixed surface are obtained. Moreover, the image force of PQC bi-material composite space is also taken into account. By virtue of numerical examples, we further revealed the electro-elastic and phonon–phason coupled properties of PQC, and the variation laws between material properties and image force. We discovered that the material parameters and loading scheme have more obvious effects on image force. The influences of multiple loads, such as line force, dislocation, and charge, on displacements and stresses are analyzed in detail. Some valuable conclusions are as follows:

(1) The image force attracts the dislocations to the surface when the boundary condition is traction-free and electrically open, while separates the dislocations from the surface when the boundary is fixed and electrically closed.
(2) The phonon force has no effect on the image force for different kinds of materials, such as crystals, piezoelectric materials, and PQCs, while the loading condition has significant effect on the image force.
(3) The image force F of bi-material is independent on the phonon–phason coupling constant R_2 and the piezoelectric constant d_{123}.

Wang and Zhong [42] investigated a line dislocation near a semi-infinite crack due to the presence of the free surface in a decagonal QC. Jiang and Liu [43] discussed the influences of the wedge angle and dislocation location on the image force for 1D hexagonal PQC. Referring to Ref.[44], with the aid of the conformal mapping method, the theory and results presented here are helpful for settling a conventional Griffith crack with traction-free or fixed boundaries. In addition, the models and method can be extended to theoretical analysis of other QCs, such as 1D and 2D QCs, even more complicated problems.

Acknowledgements This work was supported by the National Natural Science Foundation of China (Grant Nos. 12272402, 11972365, and 12102458) and China Agricultural University Education Foundation (No. 1101-2412001).

Data availability The data generated or analyzed used to support the findings of this study are included within the article.

Appendix

By using Eqs. (1), (2), and (3), we have

$$\mathbf{Q}=\begin{bmatrix} C_{11} & 0 & 0 & R_1 & 0 & 0 & 0\\ 0 & C_{44} & 0 & 0 & R_3 & 0 & 0\\ 0 & 0 & C_{44} & 0 & 0 & R_3 & 0\\ R_1 & 0 & 0 & K_{11} & 0 & 0 & 0\\ 0 & R_3 & 0 & 0 & K_{44} & 0 & 0\\ 0 & 0 & R_3 & 0 & 0 & K_{44} & 0\\ 0 & 0 & 0 & 0 & 0 & 0 & -\xi_{11} \end{bmatrix}, \mathbf{R}=\begin{bmatrix} 0 & 0 & C_{12} & 0 & 0 & R_2 & 0\\ 0 & 0 & 0 & 0 & 0 & 0 & d_{14}\\ C_{44} & 0 & 0 & R_3 & 0 & 0 & 0\\ 0 & 0 & R_2 & 0 & 0 & K_{12} & 0\\ 0 & 0 & 0 & 0 & 0 & 0 & d_{123}\\ R_3 & 0 & 0 & K_{44} & 0 & 0 & 0\\ 0 & d_{14} & 0 & 0 & d_{123} & 0 & 0 \end{bmatrix},$$
$$\mathbf{T}=\begin{bmatrix} C_{44} & 0 & 0 & R_3 & 0 & 0 & 0\\ 0 & C_{44} & 0 & 0 & R_3 & 0 & 0\\ 0 & 0 & C_{11} & 0 & 0 & R_1 & 0\\ R_3 & 0 & 0 & K_{44} & 0 & 0 & 0\\ 0 & R_3 & 0 & 0 & K_{44} & 0 & 0\\ 0 & 0 & R_1 & 0 & 0 & K_{11} & 0\\ 0 & 0 & 0 & 0 & 0 & 0 & -\xi_{33} \end{bmatrix}. \tag{A1}$$

By Eq. (29), we introduced a new function

$$F^{*}=\mathrm{Re}\sum_{\beta=1}^{7}\sum_{\alpha=1}^{7}\left[\frac{p_\alpha}{p_\alpha-\overline{p}_\beta}\left(\mathbf{B}\mathbf{I}_\alpha\mathbf{B}^{-1}\right)\mathbf{L}\left(\overline{\mathbf{B}}\mathbf{I}_\beta\overline{\mathbf{B}}^{-1}\right)^{T}\right] \tag{A2}$$

For Eq. (A2), first, the right side is replaced by its complex conjugate, then the α and β are interchanged, and finally, matrix transpose is applied on the right. Based on these operations, we can obtain that Eq. (A3) is equal to Eq. (A2).

$$F^{*}=\mathrm{Re}\sum_{\beta=1}^{7}\sum_{\alpha=1}^{7}\left[\frac{-\overline{p}_\beta}{p_\alpha-\overline{p}_\beta}\left(\mathbf{B}\mathbf{I}_\alpha\mathbf{B}^{-1}\right)\mathbf{L}\left(\overline{\mathbf{B}}\mathbf{I}_\beta\overline{\mathbf{B}}^{-1}\right)^{T}\right]. \tag{A3}$$

Using Eq. (15), we get

$$\mathbf{L}-\mathbf{H}^{-1}\mathbf{S}\mathbf{S}=\mathbf{H}^{-1}. \tag{A4}$$

Since $\mathbf{H}^{-1}\mathbf{S}$ is antisymmetric, Eq. (A4) can be re-expressed as follows:

$$\mathbf{H}^{-1}-\mathbf{L}=\mathbf{S}^{T}\mathbf{H}^{-1}\mathbf{S}. \tag{A5}$$

In the above, $\mathbf{H}^{-1}$ and$\mathbf{L}$ are positive definite, while $\mathbf{S}$ is singular [40]. We can conclude that $\mathbf{H}^{-1}$-$\mathbf{L}$ is positive semi-definite.

Substituting Eqs. (37) and (38) into Eq. (36) to yield

$$\begin{aligned}
&\frac{1}{\pi}\mathrm{Im}\left[\mathbf{A}_1<\ln\left(x_1-p_\alpha^{(1)}d\right)>\mathbf{q}\right]+\frac{1}{\pi}\mathrm{Im}\sum_{\beta=1}^{7}\left[\mathbf{A}_1\left(\ln\left(x_1-\overline{p}_\beta^{(1)}d\right)\right)\mathbf{q}_\beta^{(1)}\right]=\frac{1}{\pi}\mathrm{Im}\sum_{\beta=1}^{7}\left[\mathbf{A}_2\left(\ln\left(x_1-p_\beta^{(1)}d\right)\right)\mathbf{q}_\beta^{(2)}\right],\\
&\frac{1}{\pi}\mathrm{Im}\left[\mathbf{B}_1<\ln\left(x_1-p_\alpha^{(1)}d\right)>\mathbf{q}\right]+\frac{1}{\pi}\mathrm{Im}\sum_{\beta=1}^{7}\left[\mathbf{B}_1\left(\ln\left(x_1-\overline{p}_\beta^{(1)}d\right)\right)\mathbf{q}_\beta^{(1)}\right]=\frac{1}{\pi}\mathrm{Im}\sum_{\beta=1}^{7}\left[\mathbf{B}_2\left(\ln\left(x_1-p_\beta^{(1)}d\right)\right)\mathbf{q}_\beta^{(2)}\right].
\end{aligned} \tag{A6}$$

Similar manipulation of Eq. (21), we have

$$\frac{1}{\pi}\mathrm{Im}\left[\mathbf{A}_1<\ln\left(x_1-p_\alpha^{(1)}d\right)>\mathbf{q}\right]=-\frac{1}{\pi}\mathrm{Im}\left[\overline{\mathbf{A}}_1<\ln\left(x_1-\overline{p}_\alpha^{(1)}d\right)>\overline{\mathbf{q}}\right], \tag{A7}$$

By Eqs. (A7), $(A6)_1$, and Eq. $(22)_1$, we derive

$$-\mathrm{Im}\sum_{\beta=1}^{7}\left[\overline{\mathbf{A}}_1\left(\ln\left(x_1-\overline{p}_\beta^{(1)}d\right)\right)\mathbf{I}_\beta\overline{\mathbf{q}}\right]+\mathrm{Im}\sum_{\beta=1}^{7}\left[\mathbf{A}_1\left(\ln\left(x_1-\overline{p}_\beta^{(1)}d\right)\right)\mathbf{q}_\beta^{(1)}\right]$$
$$=-\mathrm{Im}\sum_{\beta=1}^{7}\left[\overline{\mathbf{A}}_2\left(\ln\left(x_1-\overline{p}_\beta^{(1)}d\right)\right)\overline{\mathbf{q}}_\beta^{(2)}\right], \tag{A8}$$

hence, Eq. (A8) has the expression

$$\mathbf{A}_1\mathbf{q}_\beta^{(1)}+\overline{\mathbf{A}}_2\overline{\mathbf{q}}_\beta^{(2)}=\overline{\mathbf{A}}_1\mathbf{I}_\beta\overline{\mathbf{q}}. \tag{A9}$$

With the aid of Eq. $(A6)_2$, the following equation is obtained due to similarity

$$\mathbf{B}_1\mathbf{q}_\beta^{(1)}+\overline{\mathbf{B}}_2\overline{\mathbf{q}}_\beta^{(2)}=\overline{\mathbf{B}}_1\mathbf{I}_\beta\overline{\mathbf{q}}. \tag{A10}$$

Equation (A9) has an alternative expression

$$\left(\mathbf{A}_1\mathbf{B}_1^{-1}\right)\mathbf{B}_1\mathbf{q}_\beta^{(1)}+\left(\overline{\mathbf{A}}_2\overline{\mathbf{B}}_2^{-1}\right)\overline{\mathbf{B}}_2\overline{\mathbf{q}}_\beta^{(2)}=\left(\overline{\mathbf{A}}_1\overline{\mathbf{B}}_1^{-1}\right)\overline{\mathbf{B}}_1\mathbf{I}_\beta\overline{\mathbf{q}}. \tag{A11}$$

Making use of Eqs. (A10) and (A11) give

$$\left(\mathbf{A}_1\mathbf{B}_1^{-1}-\overline{\mathbf{A}}_2\overline{\mathbf{B}}_2^{-1}\right)\overline{\mathbf{B}}_2\overline{\mathbf{q}}_\beta^{(2)}=\left(\mathbf{A}_1\mathbf{B}_1^{-1}-\overline{\mathbf{A}}_1\overline{\mathbf{B}}_1^{-1}\right)\overline{\mathbf{B}}_1\mathbf{I}_\beta\overline{\mathbf{q}}, \tag{A12}$$

or

$$\left(\mathbf{M}_1^{-1}+\overline{\mathbf{M}}_2^{-1}\right)\overline{\mathbf{B}}_2\overline{\mathbf{q}}_\beta^{(2)}=2\mathbf{L}_1^{-1}\left(\overline{\mathbf{B}}_1\mathbf{I}_\beta\overline{\mathbf{q}}\right), \tag{A13}$$

where

$$\mathbf{M}=-i\mathbf{B}\mathbf{A}^{-1}=\mathbf{H}^{-1}+i\mathbf{H}^{-1}\mathbf{S},\ \mathbf{M}^{-1}=i\mathbf{A}\mathbf{B}^{-1}=\mathbf{L}^{-1}-i\mathbf{S}\mathbf{L}^{-1}. \tag{A14}$$

References

1. Barnett, D.M., Lothe, J.: An image force theorem for dislocations in anisotropic bicrystals. J. Phys. F **4**(10), 1618–1635 (1974)
2. Asaro, R.J.: Image force theorem for a dislocation near a crack in an anisotropic elastic medium. J. Phys. F **5**(12), 2249–2255 (1975)
3. Ting, T.C.T., Barnett, D.M.: Image force on line dislocations in anisotropic elastic half-spaces with a fixed boundary. Int. J. Solids Struct. **30**(3), 313–323 (1993)
4. Lubarda, V.A.: Image force on a straight dislocation emitted from a cylindrical void. Int. J. Solids Struct. **48**(5), 648–660 (2011)
5. Shechtman, D., Blech, I., Gratias, D., Cahn, J.W.: Metallic phase with long-range orientational order and no translational symmetry. Phys. Rev. Lett. **53**(20), 195l–1953 (1984)
6. Jaric, M.V., Nelson, D.R.: Introduction to quasicrystals. Phys. Today **43**(3), 77–79 (1990)
7. Guo, X.P., Chen, J.F., Yu, H.L., Liao, H.L., Coddet, C.: A study on the microstructure and tribological behavior of cold-sprayed metal matrix composites reinforced by particulate quasicrystal. Surf. Coat. Tech. **268**, 94–98 (2015)
8. Zhu, S., Yu, H.J., Hao, L.L., Wang, B., Yang, Y.N., Huang, K., Li, Z.X.: Exploring the dynamic fracture performance of epoxy/cement based piezoelectric composites with complex interfaces. Compos. Struct. **305**, 1–19 (2023)
9. Zhu, S., Yu, H.J., Wu, X.R., Hao, L.L., Shen, Z., Wang, J.S., Guo, L.C.: Dynamic fracture analysis in nonhomogeneous piezoelectric materials with a new domain-independent interaction integral. Theor. Appl. Fract. Mech. **122**, 1–17 (2022)
10. Zhu, S., Liu, H.T.: Finite element analysis of the three-dimensional crack and defects in piezoelectric materials under the electro-mechanical coupling field. J. Intel. Mat. Syst. Str. **32**(15), 1662–1677 (2021)
11. Wang, T.C.: Analysis of strip electric saturation model of crack problem in piezoelectric materials. Int. J. Solids Struct. **37**(42), 6031–6049 (2000)
12. Chen, C.D.: On the singularities of the thermo-electro-elastic fields near the apex of a piezoelectric bonded wedge. Int. J. Solids. Struct. **43**(5), 957–981 (2006)
13. Yu, H.J., Wu, L.Z., Guo, L.C., Ma, J.W.: A domain-independent interaction integral for fracture analysis of nonhomogeneous piezoelectric materials. Int. J. Solids Struct. **49**, 3301–3315 (2012)
14. Fan, C.Y., Yuan, Y.P., Pan, Y.B., Zhao, M.H.: Analysis of cracks in one-dimensional hexagonal quasicrystals with the heat effect. Int. J. Solids Struct. **120**, 146–156 (2017)

15. Guo, J.H., Yu, J., Xing, Y.M.: Anti-plane analysis on a finite crack in a one-dimensional hexagonal quasicrystal strip. Mech. Res. Commun. **52**, 40–45 (2013)
16. Zhou, Y.B., Li, X.F.: A Yoffe-type moving crack in one-dimensional hexagonal piezoelectric quasicrystals. Appl. Math. Model. **65**, 148–163 (2019)
17. Li, L.H., Cui, X.W., Guo, J.H.: Interaction between a screw dislocation and an elliptical hole with two asymmetrical cracks in a one-dimensional hexagonal quasicrystal with piezoelectric effect. Appl. Math. Mech. Engl. Ed. **41**(6), 899–908 (2020)
18. Mu, X., Xu, W.S., Zhu, Z.W., Zhang, L.L., Gao, Y.: Multi-field coupling solutions of functionally graded two-dimensional piezoelectric quasicrystal wedges and spaces. Appl. Math. Model. **109**, 251–264 (2022)
19. Zhang, L.L., Wu, D., Xu, W.S., Yang, L.Z., Ricoeur, A., Wang, Z.B., Gao, Y.: Green's functions of one-dimensional quasicrystal bi-material with piezoelectric effect. Phys. Lett. A **380**(39), 3222–3228 (2016)
20. Wu, D., Zhang, L.L., Xu, W.S., Yang, L.Z., Gao, Y.: Electroelastic Green's function of one-dimensional piezoelectric quasicrystals subjected to multi-physics loads. J. Intel. Mat. Syst. Str. **28**(12), 1651–1661 (2017)
21. Xu, W.S., Wu, D., Gao, Y.: Fundamental elastic field in an infinite plane of two-dimensional piezoelectric quasicrystal subjected to multi-physics loads. Appl. Math. Model. **52**, 186–196 (2017)
22. Gao, Y., Ricoeur, A.: Three-dimensional Green's functions for two-dimensional quasi-crystal bimaterials. P. R. Soc. A-Math. Phys. **467**(2133), 2622–2642 (2011)
23. Wang, X.: Time-harmonic dynamic Green's functions for one-dimensional hexagonal quasicrystals. Acta Mech. Solida Sin. **18**(4), 302–306 (2005)
24. Li, S., Li, L.H.: Effective elastic properties of one-dimensional hexagonal quasicrystal composites. Appl. Math. Mech.-Engl. Ed. **42**(10), 1439–1448 (2021)
25. Hwu, C., Ikeda, T.: Electromechanical fracture analysis for corners and cracks in piezoelectric materials. Int. J. Solids Struct. **45**(22–23), 5744–5764 (2008)
26. Ting, T.C.T.: The critical angle of the anisotropic elastic wedge subject to uniform tractions. J. Elast. **20**(2), 113–130 (1988)
27. Hwu, C.: Some explicit expressions of extended Stroh formalism for two-dimensional piezoelectric anisotropic elasticity. Int. J. Solids Struct. **45**(16), 4460–4473 (2008)
28. Ting, T.C.T.: Symmetric representation of stress and strain in the Stroh formalism and physical meaning of the tensors L, S, L(θ) and S(θ). J. Elast. **50**(1), 91–96 (1998)
29. Hwu, C., Ting, T.C.T.: Solutions for the anisotropic elastic wedge at critical wedge angles. J. Elast. **24**(1–3), 1–20 (1990)
30. Ting, T.C.T.: Line forces and dislocations in anisotropic elastic composite wedges and spaces. Phys. Status Solidi B **146**(1), 81–90 (1988)
31. Chung, M.Y., Ting, T.C.T.: Line force, charge, and dislocation in anisotropic piezoelectric composite wedges and spaces. J. Appl. Mech-T. ASME. **62**(2), 423–428 (1995)
32. Mu, X., Fu, X.Y., Zhu, Z.W., Zhang, L.L., Gao, Y.: Fundamental solutions of critical wedge angles for one-dimensional piezoelectric quasicrystal wedge. Appl. Math. Mech.-Engl. Ed. **43**(5), 709–728 (2022)
33. Wang, R.H., Hu, C.Z., Gui, J.N.: Quasicrystal Physics. Science Press (2004). (**in Chinese**)
34. Fan, T.Y.: Mathematical Theory of Elasticity and Relevant Topics of Solid and Soft-Matter Quasicrystals and Its Applications. Beijing Institute of Technology Press (2014)
35. Long, F., Li, X.F.: Flamant problem of a cubic quasicrystal half-plane. Z. Angew. Math. Phys. **73**(3), 1–13 (2022)
36. Long, F., Li, X.F.: Elastic field of a rotating cubic quasicrystal disk. Arch. Appl. Mech. **16**, 1–15 (2022)
37. Long, F., Li, X.F.: Thermal stresses of a cubic quasicrystal circular disc. Mech. Res. Commun. **2022**(124), 1–13 (2022)
38. Mu, X., Cao, T., Xu, W.S., Zhu, Z.W., Qin, T.Y., Zhang, L.L., Gao, Y.: Singularities of three-dimensional cubic piezoelectric quasicrystal composite wedges and spaces. Acta Mech. Solida Sin. **36**(42), 143–155 (2022)
39. Hwu, C.B.: Anisotropic Elastic Plates. Springer (2010)
40. Ting, T.C.T.: Anisotropic Elasticity: Theory and Applications. Oxford University, Oxford (1996)
41. Chen, B.J., Xiao, Z.M., Liew, K.M.: A line dislocation interacting with a semi-infinite crack in piezoelectric solid. Int. J. Eng. Sci. **42**(7), 1–11 (2004)
42. Wang, X., Zhong, Z.: Interaction between a semi-infinite crack and a straight dislocation in a decagonal quasicrystal. Int. J. Eng. Sci. **42**(5/6), 521–538 (2004)
43. Jiang, L.J., Liu, G.T.: The interaction between a screw dislocation and a wedge-shaped crack in one-dimensional hexagonal piezoelectric quasicrystals. Chin. Phys. B **26**(4), 245–251 (2017)
44. Liu, J.X., Wang, B., Du, S.Y.: Electro-elastic Green's functions for a piezoelectric half-space and their applications. Appl. Math. Mech.-Engl. Ed. **18**(11), 1–7 (1997)